EurJIC European Journal of Inorganic Chemistry

ChemPubSoc Europe

FULL PAPER

DOI:10.1002/ejic.201500884

Formation of Hybrid Guanidine-Stabilized Bis(μ-oxo)-dicopper Cores in Solution: Electronic and Steric Perturbations

Sonja Herres-Pawlis,*[a] Roxana Haase,[b] Pratik Verma,[c] Alexander Hoffmann,[a] Peng Kang,[c] and T. Daniel P. Stack*[c]

Keywords: Bioinorganic chemistry / Enzyme models / Copper / Bridging ligands / Density functional calculations

A series of new hybrid peralkylated amine-guanidine ligands based on a 1,3-propanediamine backbone and their Cu-O_2 chemistry is reported. The copper(I) complexes react readily with O_2 at low temperatures in aprotic solvents with weakly coordinating anions to form exclusively bis(μ-oxo)dicopper species (**O**). Variation of the substituents on each side of the hybrid bidentate ligand reveal that less sterically demanding amine and guanidine substituents increase not only the thermal stability of the formed **O** cores but also enhance inner-sphere phenolate hydroxylation pathways. TD-DFT analysis on selected guanidine-amine **O** species suggest that the additional visible-wavelength feature observed is a guanidine $\pi^* \rightarrow Cu_2O_2$ LMCT, which appears along with the classic oxo-$\sigma_u^* \rightarrow Cu^{III}$ and $\pi_\sigma^* \rightarrow Cu^{III}$ LMCT transitions.

Introduction

Many copper enzymes in nature directly activate O_2 to perform a myriad of essential chemical transformations that are almost exclusively performed with this metal.[1–6] Tyrosinases (Ty), which are ubiquitous in both eukaryotes and prokaryotes, are well recognized examples that perform the first committed step in the synthesis of melanin from tyrosine by catalytic hydroxylation of the phenol to a catechol.[4–6] Recent crystal structures of oxygenated tyrosinase (oxyTy) confirmed a binuclear copper(II) μ-η^2:η^2-peroxo species (**^{S}P**),[7] which was anticipated from earlier spectroscopic and modeling studies.[6] Given the unique and impressive catalytic oxidation chemistry of tyrosinases, decades of effort have been directed towards reproducing their reversible dioxygen binding and oxidative reactivity in small synthetic complexes.[1–6,8–15] Synthetic ligand systems that integrate electron-rich amine ligating groups in place of imidazoles can form side-on peroxide species exclusively, but more commonly an isomeric species, a bis-oxide-bis-Cu^{III} complex (**O**), is formed, presumably due to the stronger σ-donating character of the amines compared with imidazole nitrogen ligating groups.[8,9,16] In a limited number of cases, the side-on peroxide and bis-oxide species exist in facile equilibrium at low temperatures, which supports the notion that the energetic difference between the two isomeric forms can be small.[8,17] In fact, the position of such equilibria is sensitive to the nature of weakly coordinating counter-anions in solution; full conversion of an optically pure **O** species with SbF_6 counter-anions into a **^{S}P** species is possible by the simple addition of one equivalent of a more coordinating anion, consistent with specific anionic binding to the less-compact **^{S}P** species.[18,19] Given that the position of this equilibrium is sensitive to anions, it is not surprising that phenolate ligation to a **^{S}P** species is capable of triggering isomerization to an **O** species with a phenolate bonded in an equatorial position. Such positioning can lead to phenol hydroxylation.[20–22] As optically characterized **O**[20–25] and **^{S}P** species[26–38] are reported with hydroxylating reactivity, it is unknown whether a single species is the hydroxylating agent or whether both are capable of such oxidation reactions.

The nature of the nitrogen ligand plays a key function in determining whether an **O** or **^{S}P** isomer is formed.[1–6,8–15] Many ligand families such as tris(pyrazolyl)borates,[39] poly(pyrazolyl)methanes,[35,40,41] alkylamines,[9,42] pyridines,[43] ketiminates,[44] guanidines,[24,45–50] and now histamines[51,52] have been investigated. Electron-rich bidentate ligands capable of adopting a planar, four-coordinate d^8 Cu^{III} center generally stabilize an **O** species if sufficient steric demand exists in the ligand framework to prevent formation of an unreactive copper(I) bis-chelated complex.[53,54] Exclusive primary amine ligation is now known to stabilize **O** species,

[a] Lehrstuhl für Bioanorganische Chemie, RWTH Aachen University,
Landoltweg 1, 52074 Aachen, Germany
E-mail: sonja.herres-pawlis@ac.rwth-aachen.de
www.bioac.ac.rwth-aachen.de
[b] Department Chemie, Anorganische Chemie, Universität Paderborn,
33098 Paderborn, Germany
[c] Department of Chemistry, Stanford University,
Stanford, California 94305, USA
E-mail: stack@stanford.edu
http://stacklab.stanford.edu/

Supporting information for this article is available on the WWW under http://dx.doi.org/10.1002/ejic.201500884.

albeit formed through a core capture synthesis rather than direct oxygenation of a copper(I) precursor.[55] In the best case, the ideal precursor copper(I) complexes are three-coordinate with a weakly associated anion or solvent molecule (e.g., acetonitrile). Such complexes allow for facile access of O_2 to the copper center and rapid dimerization to an **O** species. The resulting **O** species are very compact, with Cu–Cu distances in the range of 2.73–2.85 Å.[53,54]

In an earlier study,[24] we compared the hybrid bidentate chelates containing one basic guanidine donor in combination with a tertiary amine to their symmetric bis-guanidine and bis-alkylated amine parental ligands. All these Cu^I complexes oxygenate to **O** species, yet only the hybrid ligand exhibited hydroxylation of phenolates at low temperature; the other complexes only exhibited radical phenolate-coupling or ligand self-oxidation. A subtle balance exists between phenolate hydroxylation, which is presumably an inner-sphere process, and phenoxyl radical chemistry. In the present study, a series of seven hybrid ligand Cu^I complexes based on a 1,3-propanediamine backbone are investigated for their reactivity with dioxygen. Systematic variation of the guanidine and amine substituents on the ligands highlights their influence on the donor capacity and optical spectroscopy along with probing the role of steric demands on the oxidation of phenolate substrates.

Results

Ligand Synthesis

The guanidine-amine-hybrid ligands ^{1}**L**–^{7}**L** (Scheme 1 and Table 1) were synthesized by conversion of an amine into a guanidine through the reaction with a chloroformamidinium chloride (Scheme 2), which is accessible in good yields from the appropriately substituted urea and phosgene.[56,57] The copper(I) complexes [**1a**]$^+$–[**7a**]$^+$, with the general formula $[(\mathbf{L})Cu^I]^{1+}$ (**L** = ^{1}**L**–^{7}**L**, Table 1), were available directly by reacting equimolar amounts of $[Cu^I(MeCN)_4]^{1+}$ and the ligand in MeCN under N_2 at ambient temperature (r.t.). The triflate counteranion ($CF_3SO_3^-$) was used throughout this study unless indicated otherwise.

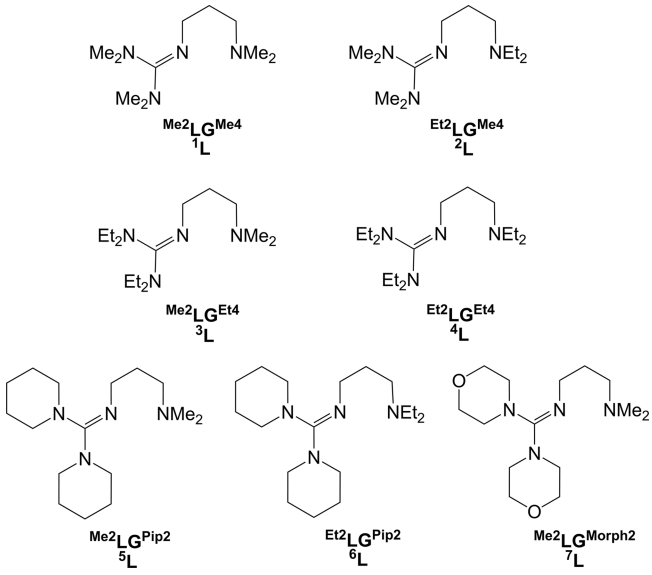

Scheme 1. Guanidine-amine hybrid ligands ^{1}**L**–^{7}**L**.

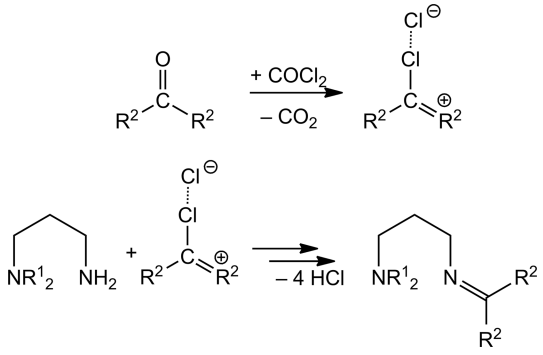

Scheme 2. Synthesis of ^{2}**L**–^{5}**L**.

Table 1. Nomenclature of ligands and Cu complexes for this study.

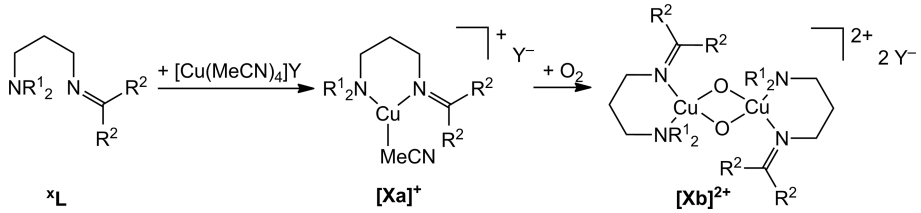

	R^1	R^2	L	$[(L)Cu^I]^+$	$[(L)_2Cu^{III}_2(\mu\text{-}O)_2]^{2+}$
^{Me2}**LG**^{Me4}	Me	NMe_2	^{1}**L**	[**1a**]$^+$	[**1b**]$^{2+}$
^{Et2}**LG**^{Me4}	Et	NMe_2	^{2}**L**	[**2a**]$^+$	[**2b**]$^{2+}$
^{Me2}**LG**^{Et4}	Me	NEt_2	^{3}**L**	[**3a**]$^+$	[**3b**]$^{2+}$
^{Et2}**LG**^{Et4}	Et	NEt_2	^{4}**L**	[**4a**]$^+$	[**4b**]$^{2+}$
^{Me2}**LG**^{Pip2}	Me	$N(CH_2)_5$	^{5}**L**	[**5a**]$^+$	[**5b**]$^{2+}$
^{Et2}**LG**^{Pip2}	Et	$N(CH_2)_5$	^{6}**L**	[**6a**]$^+$	[**6b**]$^{2+}$
^{Me2}**LG**^{Morph2}	Me	$N(CH_2)_4O$	^{7}**L**	[**7a**]$^+$	[**7b**]$^{2+}$

Oxygenation of $[1a]^+$–$[7a]^+$

Concentrated solutions of $[1a]^+$–$[7a]^+$ prepared in situ were injected into preoxygenated solvents (1 atm O_2) to generate $[1b]^{2+}$–$[7b]^{2+}$ ([Cu] = 0.5–4 mM), which all possess intense charge transfer (CT) bands near 300 and 400 nm ($\varepsilon \approx 16\ mM^{-1}cm^{-1}$/Cu-dimer) and a weaker CT band near 440 nm ($\varepsilon \approx 8\ mM^{-1}cm^{-1}$) (Figure 1, Table 2). The similarities of the absorption band shapes and intensities of $[1b]^{2+}$, a previously characterized **O** species with exclusive guanidine ligation,[24] to those of $[2b]^{2+}$–$[7b]^{2+}$ are consistent with exclusive **O** species formation. The incorporated O_2 in $[2b]^{2+}$–$[7b]^{2+}$ is not removed by cycles of evacuation and purging with N_2, in line with the physical attributes of $[1b]^{2+}$ and other **O** species.[23,24,49,58] The visible CT bands of $[3b]^{2+}$ and $[4b]^{2+}$ are more distinct and intense than those of $[1b]^{2+}$ and $[2b]^{2+}$.

Spectrophotometric Titrations with Ferrocene Monocarboxylic Acid

The extent of **O** species formation of $[1b]^{2+}$, $[3b]^{2+}$, $[5b]^{2+}$, and $[7b]^{2+}$ was quantified by spectrophotometric titrations using ferrocene monocarboxylic acid (FcCOOH), which is a method that has been validated by titration of other **O** species, for example $[1b]^{2+}$.[24] FcCOOH is a one-electron, one-proton donor with a weak OH bond dissoci-

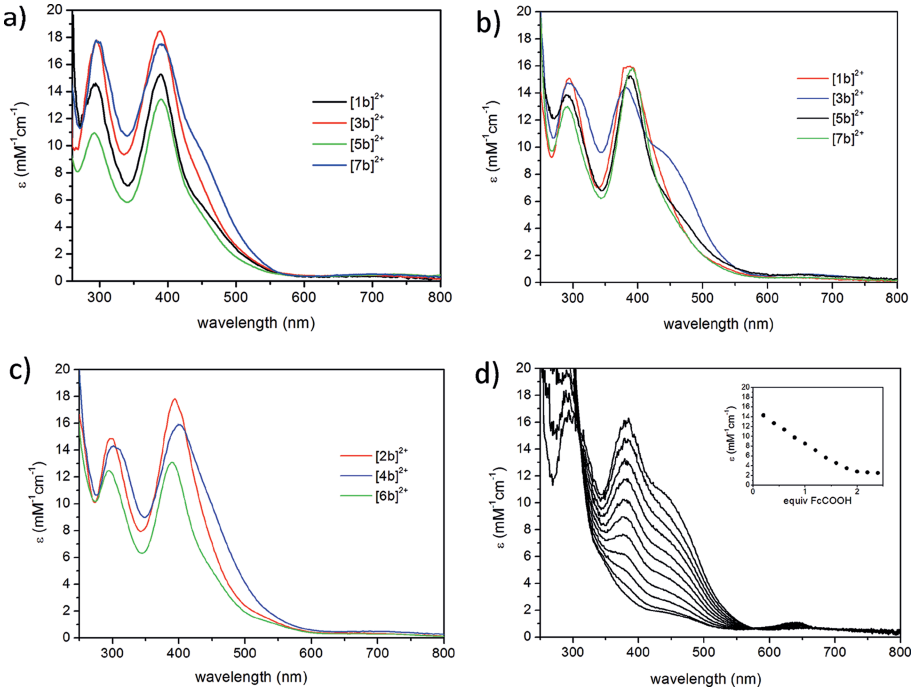

Figure 1. (a) Solution UV/Vis spectra of $[1b]^{2+}$, $[3b]^{2+}$, $[5b]^{2+}$, and $[7b]^{2+}$ ([Cu] = 1 mM, THF, 195 K, $\varepsilon\ mM^{-1}cm^{-1}$/dimer, $CF_3SO_3^-$); (b) Solution UV/Vis spectra of $[1b]^{2+}$, $[3b]^{2+}$, $[5b]^{2+}$, and $[7b]^{2+}$ ([Cu] = 1 mM, THF, 195 K, $\varepsilon\ mM^{-1}cm^{-1}$/dimer, SbF_6^-); (c) Solution UV/Vis spectra of $[2b]^{2+}$, $[4b]^{2+}$, and $[6b]^{2+}$ ([Cu] = 1 mM, THF, 195 K, $\varepsilon\ mM^{-1}cm^{-1}$/dimer, $CF_3SO_3^-$); (d) Titration of $[3b](SbF_6)_2$ in 0.2 equiv. steps with ferrocene monocarboxylic acid (FcCOOH) at 195 K in THF. The 635 nm absorption feature is associated with ferrocenium carboxylate. Inset: extinction coefficient at 389 nm vs. the number of equiv. of FcCOOH per dimer.

Table 2. UV/Vis features,[a] thermal decomposition data, and extent of formation of $[1b]^{2+}$–$[7b]^{2+}$.

	Counter anaion	λ (nm) [ε ($mM^{-1}cm^{-1}$)]	Formation[b] [%]	Decay rate, 253 K k_{obs} (s^{-1}) [$t_{1/2}$ (s)]	$\Delta H^{\ddagger}$ (kcal mol^{-1}) [$\Delta S^{\ddagger}$ (cal K^{-1} mol^{-1})]	Iodoform test
$[1b]^{2+}$	$CF_3SO_3^-$	297 [20], 385 [18], 430 [8]	> 95	1.3×10^{-3} [790]	11.5(3) [–26(1)]	negative
	SbF_6^-	290 [11], 386 [10], 430 [7]	n/a	1.5×10^{-3} [660]	13.4(1) [–18(5)]	n/a
$[2b]^{2+}$	$CF_3SO_3^-$	297 [15], 392 [18], 435 [9]	n/a	6.6×10^{-2} [15][c]	6.5(5) [–38(3)]	positive
$[3b]^{2+}$	$CF_3SO_3^-$	295 [18], 389 [17], 456 [9]	> 95	2.2×10^{-3} [460]	12.4(3) [–21(1)]	negative
	SbF_6^-	296 [15], 383 [14], 448 [9]	> 95	n/a	n/a	n/a
$[4b]^{2+}$	$CF_3SO_3^-$	302 [14], 399 [16], 450 [10]	n/a	0.12 [9][c]	5.5(5) [–41(3)]	positive
$[5b]^{2+}$	$CF_3SO_3^-$	293 [14], 388 [14], 435 [7]	n/a	n/a	n/a	n/a
	SbF_6^-	290 [14], 387 [15], 461 [5]	70	n/a	n/a	n/a
$[6b]^{2+}$	$CF_3SO_3^-$	295 [12], 390 [13], 430 [7]	n/a	0.11 [9][c]	7.4(5) [–33(3)]	positive
$[7b]^{2+}$	$CF_3SO_3^-$	292 [11], 393 [13], 430 [7]	80	5.9×10^{-3} [170][c]	2.6(7) [–59(4)]	n/a
	SbF_6^-	290 [13], 392 [16], 458 [4]	n/a	n/a	n/a	n/a

[a] λ_{max} (nm) [ε ($mM^{-1}cm^{-1}$)/Cu-dimer] at 195 K without solvent contraction corrections from 298 to 195 K (ca. 10%), the band position and intensity was determined by Gaussian deconvolution. [b] Determined by back-titration with FcCOOH. [c] Extrapolated from the Eyring data.

ation energy (BDE, 72 kcal mol^{-1}).[24] Two equivalents are required to convert an **O** species stoichiometrically into the corresponding bis(μ-hydroxo)dicopper complex, which is the presumed thermodynamic product.[24] Titrations were monitored by the disappearance of the LMCT features near 400 nm because neither the resulting copper products nor the ferrocenium carboxylate product absorb appreciably in that range (Figure 1, d).

Optical titrations of [**3b**]$(CF_3SO_3)_2$ with FcCOOH required slightly more than 1.9 equiv. per dimer and showed a linear change of absorbance with added titrant under anaerobic conditions (Figure S1); more than 2 equiv. was required when excess dioxygen was not removed. Titration of [**3b**]$(CF_3SO_3)_2$ compared with [**3b**]$(SbF_6)_2$ required five times longer to achieve equilibrium in each step; in general, the $CF_3SO_3^-$ salts required longer equilibration times. Titrations indicated more than 95% formation of [**3b**]$(CF_3SO_3)_2$ and [**3b**]$(SbF_6)_2$ and 80% formation of [**7b**]$^{2+}$ (Figure S2). Similar titrations of [**1b**]$^{2+}$ previously indicated more than 95% formation. Complexes [**2b**]$^{2+}$, [**4b**]$^{2+}$, and [**6b**]$^{2+}$ were not titrated with FcCOOH because their thermal decays at 195 K are significant in the required titration time.

Thermal Decomposition in Solution

The thermal decomposition kinetics of [**1b**]$^{2+}$–[**7b**]$^{2+}$ were studied by UV/Vis spectroscopy. Solutions of [**1b**]$^{2+}$–[**7b**]$^{2+}$ ([Cu] ca. 1–2 mM, tetrahydrofuran (THF), 195 K) were formed as described above and the excess O_2 was removed by cycles of evacuation and purging with N_2. Each solution was warmed rapidly to a set temperature, and the time-dependent evolution of optical features at a single wavelength was analyzed to provide a decomposition rate constant (k_{obs}). The decay activation parameters from an Eyring analysis in the 213–273 K range (Table 2) support the conclusion that thermal decomposition is not influenced significantly by the choice of counter-anions; for example, similar activation parameters of [**1b**]$(CF_3SO_3)_2$ and [**1b**]$(SbF_6)_2$ in THF were measured.[24]

The thermal decay products of [**1b**]$^{2+}$–[**7b**]$^{2+}$ were analyzed by GC and GC–MS, after an aqueous work-up. The parent ion of the intact ligand was not observed but unidentified fragments of low molecular weight were observed. Dealkylation of amine ligating groups is a common thermal decay pathway for **O** complexes.[16,58–60] Indeed, ligand de-ethylation could be inferred through the iodoform colorimetric analysis for acetaldehyde.[61] Complexes [**2b**]$^{2+}$, [**4b**]$^{2+}$, and [**6b**]$^{2+}$, containing NEt_2 groups, gave a positive iodoform test, whereas [**1b**]$^{2+}$ and [**3b**]$^{2+}$, with NMe_2 groups, gave a negative test. Given that [**3b**]$^{2+}$ with NMe_2 and ethyl substitutents on the guanidine subunit gave a negative test, it can be concluded that de-ethylation occurs from an amine NEt_2 group. The activation enthalpies of NMe_2 containing complexes, [**1b**]$^{2+}$ and [**3b**]$^{2+}$, are significantly higher than those for NEt_2 containing complexes, [**2b**]$^{2+}$ and [**4b**]$^{2+}$, which is consistent with the weaker methylene C–H BDE of a NEt_2 group.

Theoretical Investigation

The ligand-to-metal charge-transfer (LMCT) features in the visible range of [**1b**]$^{2+}$–[**7b**]$^{2+}$ are sensitive to the steric demands of the guanidine alkyl substitutents, presumably arising from differential orientation of the guanidine planes relative to the Cu_2O_2 core. The intra-guanidine twists, the dihedral angles between the four-atom $N_{amine}C_3$ planes and the four atom $C_{gua}N_3$ plane (Figure 2, a), are observed in the X-ray crystal structures of both metal-coordinated guanidines[47,62] and uncoordinated guanidines.[63,64] These twists result from steric interactions between adjacent guanidine NMe_2 groups. Smaller twists allow for greater delocalization and stabilization of the guanidine π system.

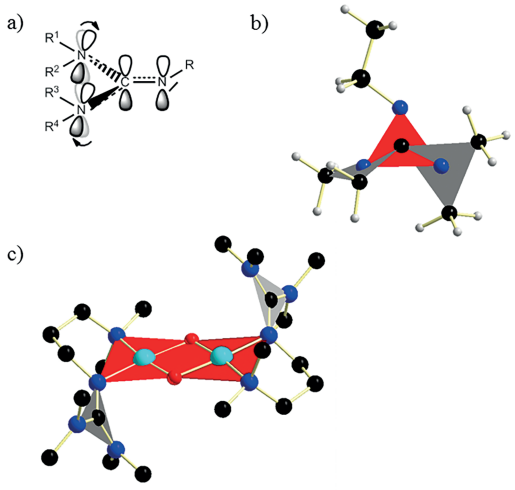

Figure 2. (a) Schematic representation of the p-orbitals forming the π-system within a guanidine group; (b) The two intra-guanidine dihedral angles (twist angles) in tetramethylguanidine ethane defined by the intersection of the planes marked in red (CN_3) and grey (NC_3); (c) Dihedral angle of the guanidine plane against the Cu_2O_2 plane in [**1b**]$^{2+}$ (CN_3 vs. Cu_2O_2).

The interplay of these twist angles with metal ligation of the guanidine nitrogen impacts the electronic communication between the guanidine π-system and the copper centers. DFT calculations at the B3LYP/2z level of theory reproduce the experimental bond lengths and trends in key metrical parameters observed among the guanidine/amine **O** complexes,[24,50] thus similar constrained optimization calculations were performed with fixed N=C–N–C(Me) dihedral angles between 10 and 50° for [**1b**]$^{2+}$. The metrical parameters for five conformers are collected in Table 3.

The fixed N=C–N–C dihedral angles within the guanidine units induce structural changes in the copper coordination and the Cu_2O_2 core. With increasing dihedral angle (i) the Cu–N_{gua} bond length increases, (ii) the Cu–N_{amine} bond shortens, (iii) the Cu···Cu vector shortens, (iv) the C=N bond length shortens, and (v) the C–$N_{gua,amine}$ bonds elongate. Accordingly, delocalization within the guanidine unit increases with decreasing guanidine twist, which is manifested in a lengthening of the C=N double bond. TD-DFT calculations on each conformer predict electronic LMCT transitions of high intensity near 300 nm, coinciding

Table 3. Metrical parameters[a] for constrained optimizations of $[\mathbf{1b}]^{2+}$.

N=C–N–C angle[b]	10°	20°	30°	40°	50°
Cu–N_{gua}	1.90	1.91	1.91	1.91	1.91
Cu–N_{amine}	2.01	2.01	2.01	2.00	1.99
Cu–Cu	2.77	2.77	2.77	2.76	2.76
C_{gua}=N_{gua}	1.37	1.36	1.35	1.34	1.33
C_{gua}–$N_{gua,amine}$	1.36	1.36	1.36	1.36	1.37
CN_3 vs. Cu_2O_2	78.8	77.4	74.6	74.1	72.8
CN_3 vs. NC_3	8.8, 11.3	18.9, 21.2	29.2, 30.9	39.8, 40.2	50.5, 49.5
NC_3 vs. NC_3	17.8	34.9	51.2	66.7	81.6
E_{elec} (kcal mol^{-1})[c]	23	11	2	3	11

[a] Distances in Å, angles in deg. [b] Fixed intra-guanidine dihedral angle. [c] Electronic energy of each conformer with the fully optimized structure selected with a N=C–N–C dihedral angle of 33.5° as the reference state.

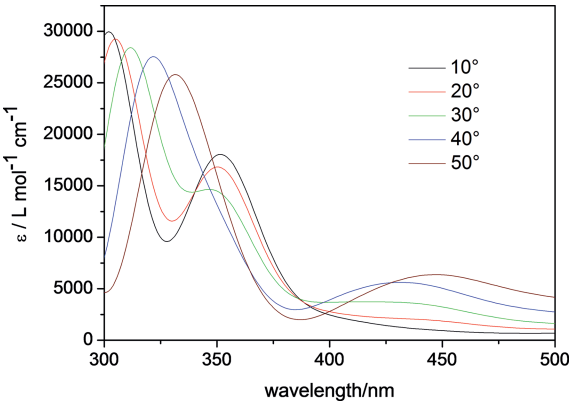

Figure 3. TD-DFT calculated UV/Vis spectra for five conformers of $[\mathbf{1b}]^{2+}$ (B3LYP/3z).

with an oxo-π*→Cu_2O_2 transition (Table 4 and Figure 3). These features undergo a significant redshift with increasing guanidine twist, along with emergence of an additional feature in the visible range near 450 nm.

Table 4. Optical transition predictions for $[\mathbf{1b}]^{2+}$ in nm.[65]

Twist	oxo-π*→Cu_2O_2 (oscillator strength)	oxo-σ*→Cu_2O_2 (oscillator strength)	π^*_{gua}→Cu_2O_2 (oscillator strength)
10°	302 (0.41)	352 (0.24)	443 (0.01)
20°	304 (0.40)	351 (0.22)	443 (0.02)
30°	311 (0.38)	348 (0.18)	443 (0.04)
40°	318 (0.29)	349 (0.13)	443 (0.06)
50°	331 (0.22)	349 (0.11)	451 (0.07)

The features near 300 and 350 nm correspond to the classical transitions of an **O** species (oxo-σ_u*→Cu^{III} and π_σ*→Cu^{III} LMCT).[24,66] The accepting molecular orbitals (LUMO and LUMO+1) are best understood as the antibonding combination of the ligand σ-bonding interactions, including both oxygen and the nitrogen atoms with the copper d_{xy} orbitals. The transitions are not altered in overall character with twisting, but redshift due to lower accepting and raised donating orbital energies, both of which result from weakened guanidine bonding to the copper centers (Figure 4). This reduced donation correlates to a smaller calculated proton affinity for the free ^{1}**L** in the constrained conformation for each twist angle.

The new LMCT absorption feature near 450 nm involves a guanidine π* orbital to LUMO+1 transition. At a 10° twist angle, this transition has limited intensity, but this increases with greater localization of the guanidine π-system associated with a greater twist. The increase in the guanidine N 2p character in the donor MO and in the overlap with the Cu_2O_2 core accepting molecular orbital allow greater absorption intensity.[67,68] The redshift of the transition appears to result primarily from a stabilization of the LUMO+1 accepting orbital.

Tetraethylguanidine units have a significant impact on the spectroscopic features of the resulting **O** species compared with tetramethylguanidine units, presumably because

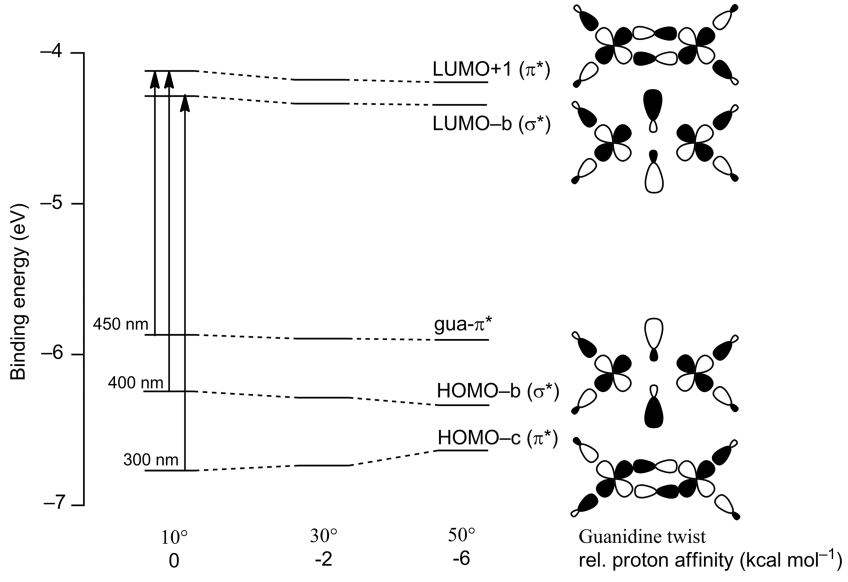

Figure 4. Molecular orbitals of twisted $[\mathbf{1b}]^{2+}$ (B3LYP/2z); a negative proton affinity implies a more acidic guanidine nitrogen.[69]

of the larger guanidine twist angles in the lower energy conformation. Unfortunately, no single crystal X-ray structure of a copper complex with a tetraethylguanidine unit is available to provide a structural benchmark for the twist angles or conformation of the ethyl substituents. Computationally, the lowest energy conformation of $[\mathbf{3b}]^{2+}$ found is correlated with the smallest average guanidine twist of 38°, which is greater than that found for the most stable conformation of $[\mathbf{1b}]^{2+}$ at 33.5°. The redshifting of the experimental and computational spectra of $[\mathbf{3b}]^{2+}$ relative to that of $[\mathbf{1b}]^{2+}$ support a greater twist angle in the former.

Reactivity with Phenolates

The oxidative reactivity of $[\mathbf{1b}]^{2+}$, $[\mathbf{3b}]^{2+}$, $[\mathbf{5b}]^{2+}$, and $[\mathbf{7b}]^{2+}$ was examined with 2,4-di-*tert*-butylphenolate (2 equiv.). The reactions were monitored optically at 195 K until either the characteristic CT feature near 400 nm was quenched or 6 h had elapsed. After acidic workup, the organic products were assayed by ^{1}H NMR spectroscopy, yields are indicated with respect to oxidizing equivalents of Cu_2O_2 core, assuming exclusive cupric products (Table 5). The fast unimolecular oxidative thermal decay of $[\mathbf{2b}]^{2+}$, $[\mathbf{4b}]^{2+}$, and $[\mathbf{6b}]^{2+}$ at 195 K precluded meaningful reactivity studies with phenolates. $[\mathbf{1b}]^{2+}$ reacted readily with 2,4-di-*tert*-butylphenolate yielding 70% of the oxygenated product 3,5-di-*tert*-butylcatechol (DBCat).[24] Small amounts of the corresponding quinone (DBQ) were also isolated. Similar oxidative behavior was observed for $[\mathbf{3b}]^{2+}$. In case of $[\mathbf{5b}]^{2+}$, the yield of the catechol decreased to 10%. By using $[\mathbf{7b}]^{2+}$, the yield of oxidized products was low and significant amounts of the radical coupled bis-phenol product (CP) formed.

Table 5. Reactivity of selected **O** species with 2,4-di-*tert*-butylphenolate.

O species	Yield [%]	Ratio of products[a] DBCat/DBQ/CP
$[\mathbf{1b}](CF_3SO_3)_2$	70	90:10:0
$[\mathbf{1b}](SbF_6)_2$	70	95:5:0
$[\mathbf{3b}](CF_3SO_3)_2$	65	90:10:0
$[\mathbf{3b}](SbF_6)_2$	80	80:20:0
$[\mathbf{5b}](CF_3SO_3)_2$	10	90:5:5
$[\mathbf{5b}](SbF_6)_2$	20	80:10:10
$[\mathbf{7b}](CF_3SO_3)_2$	30	60:10:30
$[\mathbf{7b}](SbF_6)_2$	40	65:10:25

[a] Yield and product ratios determined based on ^{1}H NMR spectroscopic analysis of the products obtained by acid quenching using an average of at least three trials with an internal standard.

Discussion

Ligand Design

The present series of hybrid guanidine ligands highlights the steric and electronic influence of the substituents on the optical spectroscopy and reactivity of formed dicopper(III)-bis(μ-oxo) species. Intraligand interactions within a guanidine unit impact the conformation of a complex, as exemplified by $[\mathbf{1b}]^{2+}$ and $[\mathbf{3b}]^{2+}$; small angular variations within the guanidine group influence its donor strength. Comparison of the 400 nm features of the **O** species formed with NMe_2- and NEt_2-containing hybrid ligands shows a clear redshift that is correlated to larger guanidine substituents ($[\mathbf{1b}]^{2+}$–$[\mathbf{4b}]^{2+}$; Table 2). An additional LMCT feature in the visible range exists for these hybrid ligand **O** species that shifts to lower energy with increasing substituent steric demand; this shift is most sensitive to the nature of the guanidine substituents.

Anion Impact

The titration of several **O** complexes with guanidine-amine hybrid ligands with ferrocene monocarboxylic acid shows clearly a near quantitative formation from their Cu^I starting materials. The FcCOOH titrations of $[\mathbf{3b}]^{2+}$, $[\mathbf{5b}]^{2+}$, and $[\mathbf{7b}]^{2+}$ suggest tight ion pairing in solution, because a change in the weakly coordinating counteranion can slow the reaction rate by up to fivefold in the case the triflate salts of $[\mathbf{1b}]^{2+}$ and $[\mathbf{3b}]^{2+}$ compared with their hexafluoridoantimonate counterparts. Assuming a direct proton coupled electron transfer (PCET) from FcCOOH to an oxygen atom of a Cu_2O_2 core, tighter anion association to the complex (e.g., triflate) should impede direct access to the core.

Thermal Decay

Whereas **O** species with NMe_2-containing ligands ($[\mathbf{1b}]^{2+}$ and $[\mathbf{3b}]^{2+}$) require higher temperatures to measure their thermal decay rates, the related complexes with Et_2N containing ligands ($[\mathbf{2b}]^{2+}$ and $[\mathbf{4b}]^{2+}$) decay with half-lives between 14 to 3 min at 193 K, depending on the guanidine substituents. Given that all decay processes fit a first-order process, it is assumed that the predominant thermal decay pathway involves intramolecular ligand oxidation, which is common among **O** species.[9,58] The systematic variation of the ligand substituents in $[\mathbf{1b}]^{2+}$–$[\mathbf{4b}]^{2+}$ correlates NEt_2 groups with lower thermal stability. De-ethylation occurs presumably through methylene hydroxylation of a NEt_2 group and release of acetaldehyde upon workup. Positive iodoform tests for acetaldehyde for the decay products of $[\mathbf{2b}]^{2+}$ and $[\mathbf{4b}]^{2+}$, but not for $[\mathbf{3b}]^{2+}$, supports selective de-ethylation of NEt_2 groups. The enhanced thermal stability of the NMe_2 containing ligands presumably results from the ca. 2–3 kcal mol^{-1} greater C–H BDE of a methylamine compared with that of a methylene C–H of an ethylamine group; selective de-ethylation of a NMeEt group from an **O** species has been reported previously.[53] Although the presence of formaldehyde was not confirmed, the presumed decay pathway for $[\mathbf{1b}]^{2+}$, $[\mathbf{3b}]^{2+}$, $[\mathbf{5b}]^{2+}$, and $[\mathbf{7b}]^{2+}$ presumably occurs by a similar hydroxylation of a NMe_2 group.

Theoretical Studies

DFT calculations on twisted congeners of $[\mathbf{1b}]^{2+}$ reveal a clear change of bonding within the guanidine group: greater

twisting results in a reduction in guanidine basicity and donating ability to the metal center. Analysis of the CT absorption feature near 450 nm by TD-DFT suggest a guanidine π* orbital to the LUMO+1 transition.[50] At a 10° twist, this guanidine π* orbital is not as pronounced as that at 50°, where this orbital gains considerable contribution due to reduced guanidine delocalization. Simultaneously, the antibonding LUMO+1 is stabilized with increasing twist due to reduced bonding and antibonding interactions, which leads to lower energy optical transitions. The increase in intensity results from the more favorable overlap of the guanidine π* orbital with the LUMO+1 orbital. Hence, the nature of the π_{gua}*-Cu_2O_2 transition leads to subtle conformational preferences of the ligands.

The DFT optimization analysis of $[\mathbf{3b}]^{2+}$ suggests greater twist angles for the guanidine units than in $[\mathbf{1b}]^{2+}$. In the absence of steric demands, a guanidine system prefers a more planar conformation and delocalization; it is the steric demands of the substituents on the guanidine that reduce this delocalization. In recent work, X-ray crystal structures of tetraethylguanidine-pyridine zinc complexes provide insights into low-energy conformers of the ligand.[62] The tetraethylguanidine systems show larger twist angles than their tetramethylguanidine counterparts. Hence, it is consistent that $[\mathbf{3b}]^{2+}$ exhibits a more intensive and more redshifted sideband ("guanidine band") than $[\mathbf{1b}]^{2+}$ in both the experimental and calculated UV/Vis spectra.

Hydroxylation Chemistry

The close similarity of the seven ligands in this investigation and the differential thermal stability and phenolate reactivity of their **O** species is striking. Although one-electron outer-sphere reduction potentials for these complexes by traditional methods are not accessible through standard low-temperature potentiometry, we assume that the ligand variations do not change significantly their thermodynamic potentials but only the kinetic barriers of different reaction pathways. Complex $[\mathbf{3b}]^{2+}$ is an efficient phenolate to catecholate hydroxylation reagent, with yields greater than 65%, comparable to other reactive **O** species.[23] Facile phenolate binding to an axial Cu^{III} position, followed by ligand rearrangement to position the phenolate in an equatorial position, and finally electrophilic attack of the phenolate π-system is one potential mechanism for hydroxylation with such an **O** species.[20–22] The significant decrease in overall catechol yield with $[\mathbf{5b}]^{2+}$ and $[\mathbf{7b}]^{2+}$ is a curious result because the attenuated yields cannot be attributed simply to increased steric demands of the ligands; although $[\mathbf{5b}]^{2+}$ and $[\mathbf{7b}]^{2+}$ do contain more atoms than $[\mathbf{3b}]^{2+}$, the effective steric demands of ethyl substituents ($[\mathbf{3b}]^{2+}$) are equivalent if not larger than for the ligands containing six-membered ring substituents when assessing the Cu_2O_2 core. Yet, in the case of $[\mathbf{5b}]^{2+}$ and $[\mathbf{7b}]^{2+}$, the percentage of radical coupled phenolates increases significantly compared with that of $[\mathbf{3b}]^{2+}$. We postulate that this differential product distribution results from reduced ligand flexibility of $[\mathbf{5b}]^{2+}$ and $[\mathbf{7b}]^{2+}$ thereby raising the ligand reorganization energy required to appropriately position a ligated phenolate for efficient hydroxylation. In these latter two cases, one-electron oxidation of the phenolate, either by an inner- or outer-sphere process, becomes competitive, releasing a phenoxyl radical, which can couple in solution.[24]

Conclusions

A series of closely related guanidine-amine hybrid ligands and their copper-dioxygen complexes provide insights into ligand design features that enhance their thermal stability so that their oxidizing capacity can be directed productively to external substrates. As previously documented and reaffirmed through this investigation, the weakest C–H bond of an alkylamine substituent that ligate a Cu^{III} center of an **O** species are oxidized readily, presumably through a hydroxylation pathway. This reactivity is understood clearly from computational studies, which identify the lowest energy C–H activation pathway along the O–O vector of the **O** Cu_2O_2 core; alkyl substituents of amines with stronger C–H BDE, such as methyl groups, provide not only enhanced thermal stability of the **O** species, but also inhibit substrate access to the core the least.[55] The guanidine stabilization of **O** species is consistent with their stronger basicity, which is greater than a peralkylated amine. Variation of guanidine substituents with associated differential twisting alters its delocalization, which impacts its ability to interact with the Cu_2O_2 core. TD-DFT calculations suggest that the new visible band in these complexes result from a CT transition from the guanidine to the Cu_2O_2 core. Finally, we suggest that phenolate hydroxylation by these hybrid-ligand **O** species requires a balance of substrate access to the Cu_2O_2 core along with ligand flexibility, because the symmetric parent ligands only exhibit radical coupling chemistry with phenolates at 195 K.[24]

Experimental Section

Caution! *Phosgene is a severe toxic agent and extensive exposure may be lethal. Use only in a well-ventilated fume hood and observe all regional regulations regarding its use.*

Materials: All manipulations were performed under pure dinitrogen (N_2), which was dried with granulate P_4O_{10}, either using Schlenk techniques or in a glovebox. Solvents (Fisher Scientific) were distilled from Na-benzophenone ketyl radical (THF, Et_2O) or from CaH_2 (MeCN, CH_2Cl_2). Dry NaH was obtained by oil removal from a 60% dispersion (Aldrich) with anhydrous hexane and dried in vacuo. $[Cu^{I}(MeCN)_4](X)$ (X = $CF_3SO_3^-$, $CH_3SO_3^-$, SbF_6^-) were prepared from Cu_2O (Aldrich) and the corresponding HX acid (Aldrich) in MeCN, and recrystallized twice from MeCN/Et_2O.[70] Ferrocene, ferrocene monocarboxylic acid and 2,4-di-*tert*-butylphenol (Aldrich) were either recrystallized or sublimed before use. Triethylamine (Fluka), and *N*^{1},*N*^{1},*N*^{3},*N*^{3}-tetramethylpropyl-1,3-diamine (Aldrich) was stored over CaH_2 and purified by flash distillation under vacuum. The chloroformamidinium chlorides *N*,*N*,*N*′,*N*′-tetramethylchloroformamidinium chloride, *N*,*N*,*N*′,*N*′-tetraethylchloroformamidinium chloride, *N*,*N*,*N*′,*N*′-dipiperidyl-

chloroformamidinium chloride, and *N*,*N*,*N*′,*N*′-dimorpholinochloroformamidinium chloride were prepared according to reported procedures.[57]

Physical Measurements: Spectra were recorded with the following spectrometers: NMR: Bruker Avance 500. IR: Nicolet P510. MS (EI, 70 eV): Saturn 2. MS (CI, CH_4): Finnigan MAT 8200. MS (ESI): Esquire 3000 Ion Trap. UV/Vis: Perkin–Elmer Lambda 45 with a low-temperature fiber-optic interface (Hellma; 1 mm), or a Cary50 with a custom-designed quartz fiber-optic dip probe (Hellma; 1 or 10 mm) and a custom-designed Schlenk cell with compression fittings (ChemGlass). Microanalyses were performed with a Perkin–Elmer 2400 analyzer.

Computational Methods: Density functional theory (DFT) calculations were performed with the Gaussian 03 program, Revision E.01.[71] The calculations of the **O** species were performed within the restricted formalism. The geometries were optimized (Table 3) using the B3LYP functional and an all electron 6-31g(d) Pople basis set on all atoms, abbreviated as 2z. The starting geometry supported by **^{1}L** was generated from its bis(μ-hydroxo)dicopper(II) X-ray crystal structure[24] by adjusting the Cu–Cu and O–O distances to 2.8 and 2.3 Å for an **O** isomer. The starting geometries for complexes with **^{3}L** were generated from [**1b**]$^{2+}$ by adding methyl groups to the guanidine substituents. Complexes [**1b**]$^{2+}$ and [**3b**]$^{2+}$ were optimized in C_i symmetry. Electronic energies were determined at the 3z level [6-311G+(d) on Cu, N and O and 6-31G(d) on C and H]; free energies were calculated from the 3z electronic energies by inclusion of the zero-point energies and thermal corrections from the frequency calculations at the 2z level, which were computed for each optimized structure to verify a true minimum.

Electronic spectra transitions were calculated using time-dependent density functional theory (TD-DFT) with the B3LYP functional and the 3z basis set using an IEF-PCM solvation model for THF (ε = 7.58) and a Pauling radii scheme. The contributions of atomic orbitals to major donor and acceptor molecular orbitals were determined by using Mulliken population analysis as implemented in AOMix[67,68] and using the NBO software as implemented in Gaussian 03, Rev. E01.[71,72] For the calculations of the relative proton affinity, an isodesmic reaction between the 50°, 30°, and 10° conformers of ligand **^{1}L** and its guanidine-protonated congeners was set up and the relative energies were calculated.[73]

General Synthesis of Guanidine-Amine Hybrid Ligands: A solution of the chloroformamidinium chloride (40 mmol) in anhydrous MeCN was added dropwise under vigorous stirring to an ice-cooled solution of the amine (40 mmol) and triethylamine (40 mmol) in anhydrous MeCN. After 3–4 h at reflux, an aqueous solution of NaOH (40 mmol) was added and the solvent and NEt_3 were evaporated under vacuum. To deprotonate the guanidine hydrochloride, 50 wt.-% KOH (aq., 15 mL) was added and the free base was extracted into the MeCN phase (3 × 30 mL). The organic phase was dried with Na_2SO_4, filtered, and removed under reduced pressure.

2-[3-(Diethylamino)propyl]-1,1,3,3-tetramethylguanidine (^{Et2}LG^{Me4}, ^{2}L): Yield 8.69 g (38.1 mmol, 95%); yellow oil. ^{1}H NMR (500 MHz, $CDCl_3$, 25 °C): δ = 0.93 (m, ^3J = 7.15 Hz, 6 H, CH_3), 1.55–1.61 (m, 2 H, CH_2), 2.39–2.45 (m, 6 H, CH_2), 2.56 (s, 6 H, CH_3), 2.65 (s, 6 H, CH_3), 3.02–3.04 (t, ^3J = 6.65 Hz, 2 H, CH_2) ppm. ^{13}C NMR (125 MHz, $CDCl_3$, 25 °C): δ = 11.8 (CH_3), 29.6 (CH_2), 38.7 (CH_3), 39.5 (CH_3), 47.0 (CH_2), 47.8 (CH_2), 50.9 (CH_2), 159.9 (C_{Gua}) ppm. EI-MS: *m*/*z* (%) = 228.2 (31) [M$^+$], 199 (63) [M$^+$ – CH_2CH_3], 157 (19), 142 (71) [M$^+$ – H_2C – $N(CH_2CH_3)_2$], 129 (46), 128 (20) [M$^+$ – $H_4C_2N(CH_2CH_3)_2$], 114 (10), 113 (14), 98 (31), 97 (44), 86 (100) [$H_2CN(CH_2CH_3)_2^+$], 85 (90), 71 (31), 58 (15), 42 (12). IR (NaCl): $\tilde{\nu}$ = 2968 (m), 2933 (m), 2871 (m), 2837 (m), 2798 (m), 1655 (w), 1624 [vs, ν(C=N)], 1496 (m), 1452 (m), 1402 (vw), 1365 (s), 1311 (vw), 1248 (w), 1234 (w), 1200 (vw), 1165 (vw), 1134 (m), 1109 (vw), 1066 (w), 1009 (vw), 991 (w), 914 (vw) cm^{-1}. $C_{12}H_{28}N_4$ (228.38): calcd. C 63.11, H 12.36, N 24.53; found C 62.88, H 12.67, N 24.81.

2-[3-(Dimethylamino)propyl]-1,1,3,3-tetraethylguanidine (^{Me2}LG^{Et4}, ^{3}L): Yield 9.12 g (35.6 mmol, 89%); yellow oil. ^{1}H NMR (500 MHz, $CDCl_3$, 25 °C): δ = 0.95–0.99 (m, 12 H, CH_3), 1.61–1.67 (m, 2 H, CH_2), 2.16 (s, 6 H, CH_3), 2.24–2.27 (m, 2 H, CH_2), 2.96 (q, ^3J = 7.1 Hz, 4 H, CH_2), 3.05–3.10 (m, 6 H, CH_2) ppm. ^{13}C NMR (125 MHz, $CDCl_3$, 25 °C): δ = 13.0 (CH_3), 13.6 (CH_3), 30.8 (CH_2), 41.5 (CH_2), 42.6 (CH_2), 45.5 (CH_3), 48.0 (CH_2), 58.4 (CH_2), 158.2 (C_{Gua}) ppm. EI-MS: *m*/*z* (%) = 256.3 (52) [M$^+$], 241 (17) [M$^+$ – CH_3], 198 (60) [M$^+$ – $H_2CN(CH_3)_2$], 185 (54), 184 (60) [M$^+$ – $H_4C_2N(CH_3)_2$], 172 (23), 127 (40), 125 (65), 114 (72), 113 (81), 100 (55), 86 (64) [$H_6C_3N(CH_3)_2^+$], 85 (72), 72 (100) [$H_4C_2N(CH_3)_2^+$], 71 (57), 70 (51), 58 (77) [$CH_2N(CH_3)_2^+$], 57 (53), 44 (41), 43 (40), 42 (41). IR (NaCl): $\tilde{\nu}$ = 2966 (s), 2931 (s), 2868 (m), 2812 (m), 2762 (m), 1610 [vs. (ν, C=N)], 1460 (m), 1402 (m), 1375 (m), 1356 (w), 1340 (w), 1302 (w), 1261 (s), 1221 (w), 1174 (vw), 1153 (vw), 1132 (m), 1097 (w), 1070 (m), 1041 (w), 1011 (vw), 968 (vw), 930 (vw) cm^{-1}. $C_{14}H_{32}N_4$ (256.43): calcd. C 65.57, H 12.58, N 21.85; found C 65.29, H 12.82, N 22.05.

2-[3-(Diethylamino)propyl]-1,1,3,3-tetraethylguanidine (^{Et2}LG^{Et4}, ^{4}L): Yield 10.64 g (37.4 mmol, 94%); yellow oil. ^{1}H NMR (500 MHz, $CDCl_3$, 25 °C): δ = 0.99–1.03 (m, 18 H, CH_3), 1.64–1.70 (m, 2 H, CH_2), 2.47–2.54 (m, 6 H, CH_2), 3.01 (q, ^3J = 7.1 Hz, 4 H, CH_2), 3.07–3.14 (m, 6 H, CH_2) ppm. ^{13}C NMR (125 MHz, $CDCl_3$, 25 °C): δ = 11.8 (CH_3), 13.0 (CH_3), 13.7 (CH_3), 29.5 (CH_2), 41.4 (CH_2), 42.7 (CH_2), 47.0 (CH_2), 48.2 (CH_2), 51.2 (CH_2), 158.3 (C_{gua}) ppm. EI-MS: *m*/*z* (%) = 284.3 (71) [M$^+$], 255 (94) [M$^+$ – CH_2CH_3], 213 (19), 198 (97) [M$^+$ – $CH_2N(CH_2CH_3)_2$], 185 (40), 184 (17) [M$^+$ – $H_4C_2N(CH_2CH_3)_2$], 182 (25), 172 (12), 156 (31), 142 (19), 127 (32), 125 (89), 114 (100) [$H_6C_3N(CH_2CH_3)_2^+$], 113 (100), 98 (50), 86 (95) [$CH_2N(CH_2CH_3)_2^+$], 85 (81), 84 (81), 72 (94) [$N(CH_2CH_3)_2^+$], 58 (37), 56 (31), 42 (21). IR (NaCl): $\tilde{\nu}$ = 2968 (vs), 2931 (s), 2870 (m), 2831 (w), 2798 (w), 1612 [vs. (ν, C=N)], 1460 (m), 1402 (m), 1375 (s), 1340 (m), 1300 (w), 1261 (s), 1221 (w), 1203 (w), 1165 (vw), 1134 (m), 1070 (m), 1011 (vw), 926 (vw), 914 (vw) cm^{-1}. $C_{16}H_{36}N_4$ (284.49): calcd. C 67.55, H 12.75, N 19.69; found C 67.59, H 12.94, N 20.03.

***N*^{1}-(Dipiperidin-1-ylmethylene)-*N*^{3},*N*^{3}-dimethylpropan-1,3-diamine (^{Me2}LG^{Pip2}, ^{5}L):** Yield 9.63 g (34.4 mmol, 86%); yellow oil. ^{1}H NMR (500 MHz, $CDCl_3$, 25 °C): δ = 1.29–1.33 (m, 12 H, CH_2), 1.44–1.50 (m, 2 H, CH_2), 1.96 (s, 6 H, CH_3), 2.05–2.08 (m, 2 H, CH_2), 2.79–2.83 (m, 8 H, CH_2), 2.90–2.92 (m, 2 H, CH_2) ppm. ^{13}C NMR (125 MHz, $CDCl_3$, 25 °C): δ = 24.6 (CH_2), 25.6 (CH_2), 30.0 (CH_2), 45.3 (CH_3), 46.8 (CH_2), 47.7 (CH_2), 48.6 (CH_2), 57.8 (CH_2), 160.0 (C_{Gua}) ppm. EI-MS: *m*/*z* (%) = 280.3 (68) [M$^+$], 265 (29) [M$^+$ – CH_3], 222 (75) [M$^+$ – $H_2CN(CH_3)_2$], 209 (38), 197 (40), 196 (80) [M$^+$ – $H_6C_3N(CH_3)_2$], 154 (15), 139 (31), 137 (61), 126 (87), 125 (78), 112 (78), 98 (15), 86 (44) [$H_6C_3N(CH_3)_2^+$], 85 (78), 84 (100) [$C_5H_{10}N^+$], 83 (32), 70 (43), 69 (88), 58 (70) [$H_2CN(CH_3)_2^+$], 56 (54), 42 (40), 41 (72). IR (NaCl): $\tilde{\nu}$ = 2933 (vs), 2854 (s), 2815 (m), 2778 (w), 1646 (s), 1614 [vs. (ν, C=N)], 1558 (w), 1442 (w), 1411 (m), 1371 (m), 1347 (vw), 1322 (vw), 1249 (s), 1213 (m), 1155 (vw), 1130 (m) cm^{-1}. $C_{16}H_{32}N_4$ (280.46): calcd. C 68.52, H 11.50, N 19.98; found C 68.34, H 11.77, N 20.31.

***N*¹-(Dipiperidin-1-ylmethylene)-*N*³,*N*³-diethylpropan-1,3-diamine (^{Et2}LG^{Pip2}, ^{6}L):** Yield 11.7 g (37.9 mmol, 95%); yellow oil. ^{1}H NMR (500 MHz, $CDCl_3$, 25 °C): δ = 0.99 (t, ^3J = 7.2 Hz, 6 H, CH_3), 1.49–1.53 (m, 12 H, CH_2), 1.61–1.66 (m, 2 H, CH_2), 2.45–2.51 (m, 6 H, CH_2), 2.93–2.95 (m, 4 H, CH_2), 3.00–3.02 (m, 4 H, CH_2), 3.12–3.15 (m, 2 H, CH_2) ppm. ^{13}C NMR (125 MHz, $CDCl_3$, 25 °C): δ = 11.9 (CH_3), 25.8 (CH_2), 26.1 (CH_2), 29.5 (CH_2), 47.0 (CH_2), 47.9 (CH_2), 48.6 (CH_2), 49.1 (CH_2), 50.9 (CH_2), 160.0 (C_{Gua}) ppm. EI-MS: *m*/*z* (%) = 308.5 (24) [M^+], 279 (28) [M^+ – CH_2CH_3], 222 (38) [M^+ – $H_2CN(CH_2CH_3)_2$], 197 (20), 196 (80), 154 (9), 137 (10), 128 (30), 126 (42), 125 (24), 113 (29), 112 (67), 86 (29) [$H_2CN(CH_2CH_3)_2^+$], 85 (53), 84 (100) [$C_5H_{10}N^+$], 69 (68), 58 (25), 41 (32). IR (NaCl): $\tilde{\nu}$ = 2968 (m), 2931 (vs), 2850 (m), 2823 (m), 1647 (m), 1616 [s (ν, C=N)], 1558 (vw), 1541 (vw), 1522 (vw), 1506 (vw), 1466 (w), 1441 (m), 1396 (m), 1369 (m), 1346 (w), 1288 (vw), 1248 (s), 1213 (m), 1157 (vw), 1130 (w), 1105 (vw), 1070 (vw), 1030 (vw), 1012 (vw), 957 (vw), 912 (w) cm^{-1}. $C_{18}H_{36}N_4$ (308.51): calcd. C 70.08, H 11.76, N 18.16; found C 69.79, H 11.84, N 18.39.

***N*¹-(Dimorpholinomethylene)-*N*³,*N*³-dimethylpropane-1,3-diamine (^{Me2}LG^{Morph2}, ^{7}L):** Yield 10.24 g (36.0 mmol, 90%); yellow oil. ^{1}H NMR (500 MHz, $CDCl_3$, 25 °C): δ = 1.63–1.69 (m, 2 H, CH_2), 2.19 (s, 6 H, CH_3), 2.26–2.29 (m, 2 H, CH_2), 3.01–3.03 (m, 4 H, CH_2), 3.12–3.14 (m, 4 H, CH_2), 3.17 (t, ^3J = 6.8 Hz, 2 H, CH_2), 3.63–3.65 (m, 8 H, CH_2) ppm. ^{13}C NMR (125 MHz, $CDCl_3$, 25 °C): δ = 30.7 (CH_2), 45.6 (CH_3), 47.5 (CH_2), 48.3 (CH_2), 58.1 (CH_2), 66.9 (CH_2), 157.5 (C_{gua}) ppm. EI-MS: *m*/*z* (%) = 284.3 (45) [M^+], 226 (64) [M^+ – $H_2CN(CH_3)_2$], 215 (18), 213 (20), 200 (18), 169 (21), 139 (32), 128 (71), 127 (48), 114 (41), 100 (19), 98 (14), 86 (66) [$H_6C_3N(CH_3)_2^+$], 85 (49), 72 (28) [$H_4C_2N(CH_3)_2^+$], 70 (71), 58 (100) [$H_2CN(CH_3)_2^+$], 42 (37). IR (NaCl): $\tilde{\nu}$ = 2956 (m), 2916 (m), 2891 (m), 2852 (s), 2765 (m), 1624 [vs. (ν (C=N)], 1539 (w), 1456 (m), 1392 (m), 1360 (m), 1300 (w), 1263 (s), 1230 (s), 1176 (w), 1147 (w), 1115 [vs. (ν, R–O–R)], 1068 (w), 1030 (m), 987 (w), 974 (w), 926 (w) cm^{-1}. $C_{14}H_{28}N_4O_2$ (284.40): calcd. C 59.12, H 9.92, N 19.70; found C 58.92, H 10.25, N 19.99.

Preparation of [(L)Cu^{I}](CF$_3$SO$_3$) and [(L)Cu^{I}](SbF$_6$) Complexes [1a]$^+$–[7a]$^+$ and of [(L)$_2$Cu$_2$O$_2$](CF$_3$SO$_3$)$_2$ and [(L)$_2$Cu$_2$O$_2$](SbF$_6$)$_2$ Complexes [1b]$^{2+}$–[7b]$^{2+}$: Solutions for optical investigations and reactivity studies of [**1b**]$^{2+}$–[**7b**]$^{2+}$ were prepared generally in situ by initially mixing equimolar amounts of [Cu^{I}(MeCN)$_4$](CF$_3$SO$_3$) or of [Cu^{I}(MeCN)$_4$](SbF$_6$), respectively, with ^{1}**L**–^{7}**L**. Oxygenation proceeded by rapid injection of a concentrated solution into preoxygenated THF at 195 K. This "injection" method allows for the fastest and most complete formation of the **O** complexes (0.1–2 mM); generally, a 10-fold dilution of the concentrated stock solution was used.

Thermal Decomposition Kinetics: The thermal decomposition reactions of [**1b**]$^{2+}$–[**4b**]$^{2+}$, [**6b**]$^{2+}$–[**7b**]$^{2+}$ were monitored in a custom-designed low-temperature cell in THF, except where otherwise noted, with [Cu] = 1.0 mM. All solutions for these studies were prepared by the "injection" method to give a final volume of 5 mL. After stabilization of the optical spectrum, the excess O_2 was removed by four cycles of vacuum/N_2 purging and the complex was allowed to decay at the desired temperature (213–273 K), which was maintained by a Lauda cryostat bath. Data collection for the decay started only after the solution had attained the desired temperature as detected by a low-temperature thermometer inserted directly into the solution; 2–3 min were normally required for thermal equilibration. The absorbance at λ_{max} of the feature near 390 nm was monitored to quantify the decay of [**1b**]$^{2+}$–[**4b**]$^{2+}$, [**6b**]$^{2+}$–[**7b**]$^{2+}$ and the data were fitted with a first-order kinetics model to obtain k_{obs} for each temperature. A minimum of five trials was conducted in each case. The activation parameters ($\Delta H^{\ddagger}$ and $\Delta S^{\ddagger}$) were obtained from an Eyring analysis of a linear fit of $\ln(k_{obs}T^{-1})$ against T^{-1} (see the Supporting Information). In a previous study, a multi-wavelength (280–450 nm) component analysis of the data for **1b** was performed by using SPECFIT and a first-order A → B reaction model was found to be suitable.[24]

Oxidation of Exogenous Substrates: The reactivity of [**1b**]$^{2+}$, [**3b**]$^{2+}$, [**5b**]$^{2+}$, and [**7b**]$^{2+}$ with exogenous substrates was monitored by following the optical decay at 195 K until no further optical change was evident or 6 h had elapsed. The 1.0 mM solutions of [**1b**]$^{2+}$, [**3b**]$^{2+}$, [**5b**]$^{2+}$, and [**7b**]$^{2+}$ were prepared in THF by bubbling O_2, and the excess O_2 was removed by purging the cell with N_2 for 15 min. Sodium 2,4-di-*tert*-butylphenolate (1–20 equiv.) was injected as a THF (0.5 mL) solution. The reactions were quenched with degassed H_2SO_4 (0.5 M, 2 mL), the volatiles were removed, the residue was extracted with CH_2Cl_2, and products were analyzed by ^{1}H NMR spectroscopy. The amounts of phenol, catechol, and quinone were quantified by comparison with authentic samples and a nonreactive internal standard. These experiments were completed at least three times for each **O** core.

Spectrophotometric titrations of [**3b**]$^{2+}$ and [**7b**]$^{2+}$ (195 K, THF, [Cu] = 1.0 mM) were conducted by successive injections of 0.2 equiv. aliquots of FcCOOH. Equilibration was assumed when successive optical spectra did not change appreciably.

Supporting Information (see footnote on the first page of this article): Eyring plots for thermal decomposition of [**2b**]$^{2+}$, [**3b**]$^{2+}$, [**4b**]$^{2+}$, [**6b**]$^{2+}$, and [**7b**]$^{2+}$, FcCOOH titration of [**3b**]$^{2+}$ and [**7b**]$^{2+}$ and input coordinates for hybrid DFT calculations.

Acknowledgments

Financial support by the Fonds der Chemischen Industrie and the Deutscher Akademischer Austauschdienst (DAAD) (fellowships to S. H.-P.), the Bundesministerium für Bildung und Forschung (MoSGrid, 01IG09006) and the Deutsche Forschungsgemeinschaft (DFG) (FOR1405; SFB749-B10) are gratefully acknowledged. S. H.-P. thanks Prof. K. Jurkschat for his valuable support. Calculation time at the ARMINIUS Cluster at the PC^2 Paderborn and the SuGI Cluster at the Regionales Rechenzentrum Köln (RRZK) is gratefully acknowledged. R. H. thanks the Evonik-Stifung for a PhD fellowship. Financial support for the work was provided by the National Institutes of Health (NIH) (GM50730, grants to P. V., P. K., and T. D. P. S.)

[1] E. I. Solomon, D. E. Heppner, E. M. Johnston, J. W. Ginsbach, J. Cirera, M. Qayyum, M. T. Kieber-Emmons, C. H. Kjaergaard, R. G. Hadt, L. Tian, *Chem. Rev.* **2014**, *114*, 3659.
[2] N. Kitajima, Y. Moro-Oka, *Chem. Rev.* **1994**, *94*, 737.
[3] M. Rolff, J. Schottenheim, H. Decker, F. Tuczek, *Chem. Soc. Rev.* **2011**, *40*, 4077.
[4] *Copper-Oxygen Chemistry* (Eds.: K. D. Karlin, S. Itoh), John Wiley & Sons, Inc., Hoboken, New Jersey, **2011**.
[5] J. P. Klinman, *Chem. Rev.* **1996**, *96*, 2541.
[6] E. I. Solomon, U. M. Sundaram, T. E. Machonkin, *Chem. Rev.* **1996**, *96*, 2563.
[7] Y. Matoba, T. Kumagai, A. Yamamoto, H. Yoshitsu, M. Sugiyama, *J. Biol. Chem.* **2006**, *281*, 8981.
[8] L. M. Mirica, X. Ottenwaelder, T. D. P. Stack, *Chem. Rev.* **2004**, *104*, 1013.
[9] T. D. P. Stack, *Dalton Trans.* **2003**, *10*, 1881.
[10] S. Itoh, S. Fukuzumi, *Acc. Chem. Res.* **2007**, *40*, 592.
[11] W. B. Tolman, *Acc. Chem. Res.* **1997**, *30*, 227.

[12] A. G. Blackman, W. B. Tolman, *Struct. Bonding (Berlin)* **2000**, *97*, 179.
[13] P. L. Holland, W. B. Tolman, *Coord. Chem. Rev.* **1999**, *192*, 855.
[14] S. Schindler, *Eur. J. Inorg. Chem.* **2000**, 2311.
[15] L. Q. Hatcher, K. D. Karlin, *Adv. Inorg. Chem.* **2006**, *58*, 131–184.
[16] J. A. Halfen, S. Mahapatra, E. C. Wilkinson, S. Kaderli, V. G. Young, L. Que Jr., A. D. Zuberbühler, W. B. Tolman, *Science* **1996**, *271*, 1397.
[17] V. Mahadevan, M. J. Henson, E. I. Solomon, T. D. P. Stack, *J. Am. Chem. Soc.* **2000**, *122*, 10249.
[18] X. Ottenwaelder, D. J. Rudd, M. C. Corbett, K. O. Hodgson, B. Hedman, T. D. P. Stack, *J. Am. Chem. Soc.* **2006**, *128*, 9268.
[19] A. K. Gupta, W. B. Tolman, *Inorg. Chem.* **2010**, *49*, 3531.
[20] L. M. Mirica, M. Vance, D. J. Rudd, B. Hedman, K. O. Hodgson, E. I. Solomon, T. D. P. Stack, *Science* **2005**, *308*, 1890.
[21] L. M. Mirica, D. J. Rudd, M. A. Vance, E. I. Solomon, K. Hodgson, B. Hedman, T. D. P. Stack, *J. Am. Chem. Soc.* **2006**, *128*, 2654.
[22] B. T. Op't Holt, M. A. Vance, L. M. Mirica, D. E. Heppner, T. D. P. Stack, E. I. Solomon, *J. Am. Chem. Soc.* **2009**, *131*, 6421.
[23] A. Company, S. Palavicini, I. Garcia-Bosch, R. Mas-Balleste, L. Que, E. V. Rybak-Akimova, L. Casella, X. Ribas, M. Costas, *Chem. Eur. J.* **2008**, *14*, 3535.
[24] S. Herres-Pawlis, P. Verma, R. Haase, P. Kang, C. T. Lyons, E. C. Wasinger, U. Flörke, G. Henkel, T. D. P. Stack, *J. Am. Chem. Soc.* **2009**, *131*, 1154.
[25] J. Becker, P. Gupta, F. Angersbach, F. Tuczek, C. Näther, M. C. Holthausen, S. Schindler, *Chem. Eur. J.* **2015**, *21*, 11735.
[26] A. Spada, S. Palavicini, E. Monzani, L. Bubacco, L. Casella, *Dalton Trans.* **2009**, 6468.
[27] S. Itoh, H. Kumei, M. Taki, S. Nagatomo, T. Kitagawa, S. Fukuzumi, *J. Am. Chem. Soc.* **2001**, *123*, 6708.
[28] L. Santagostini, M. Gullotti, E. Monzani, L. Casella, R. Dillinger, F. Tuczek, *Chem. Eur. J.* **2000**, *6*, 519.
[29] L. M. Mirica, M. Vance, D. J. Rudd, B. Hedman, K. O. Hodgson, E. I. Solomon, T. D. P. Stack, *J. Am. Chem. Soc.* **2002**, *124*, 9332.
[30] S. Palavicini, A. Granata, E. Monzani, L. Casella, *J. Am. Chem. Soc.* **2005**, *127*, 18031.
[31] C. Citek, C. T. Lyons, E. C. Wasinger, T. D. P. Stack, *Nat. Chem.* **2012**, *4*, 317.
[32] M. Réglier, C. Jorand, B. Waegell, *J. Chem. Soc., Chem. Commun.* **1990**, 1752.
[33] M. Rolff, J. Schottenheim, G. Peters, F. Tuczek, *Angew. Chem. Int. Ed.* **2010**, *49*, 6438; *Angew. Chem.* **2010**, *122*, 6583.
[34] L. Casella, M. Gullotti, R. Radaelli, P. Di Gennaro, *J. Chem. Soc., Chem. Commun.* **1991**, 1611.
[35] A. Hoffmann, C. Citek, S. Binder, A. Goos, M. Rübhausen, O. Troeppner, I. Ivanović-Burmazović, E. C. Wasinger, T. D. P. Stack, S. Herres-Pawlis, *Angew. Chem. Int. Ed.* **2013**, *52*, 5398; *Angew. Chem.* **2013**, *125*, 5508.
[36] A. Hoffmann, S. Herres-Pawlis, *Chem. Commun.* **2014**, *50*, 403.
[37] J. N. Hamann, F. Tuczek, *Chem. Commun.* **2014**, *50*, 2298.
[38] J. Schottenheim, N. Fateeva, W. Thimm, J. Krahmer, F. Tuczek, *Z. Anorg. Allg. Chem.* **2013**, *8*, 1491.
[39] N. Kitajima, K. Fujisawa, Y. Moro-oka, K. Toriumi, *J. Am. Chem. Soc.* **1989**, *111*, 8975.
[40] M. Cvetkovic, S. R. Batten, B. Moubaraki, K. S. Murray, L. Spiccia, *Inorg. Chim. Acta* **2001**, *324*, 131.
[41] K. Fujisawa, T. Ono, Y. Ishikawa, N. Amir, Y. Miyashita, K.-I. Okamoto, N. Lehnert, *Inorg. Chem.* **2006**, *45*, 1698.
[42] M. J. Henson, V. Mahadevan, T. D. P. Stack, E. I. Solomon, *Inorg. Chem.* **2001**, *40*, 5068.
[43] T. Osako, K. Ohkubo, M. Taki, Y. Tachi, S. Fukuzumi, S. Itoh, *J. Am. Chem. Soc.* **2003**, *125*, 11027.
[44] D. J. E. Spencer, A. M. Reynolds, P. L. Holland, B. A. Jazdzewski, C. Duboc-Toia, L. Le Pape, S. Yokota, Y. Tachi, S. Itoh, W. B. Tolman, *Inorg. Chem.* **2002**, *41*, 6307.
[45] D. Petrovic, L. M. R. Hill, P. G. Jones, W. B. Tolman, M. Tamm, *Dalton Trans.* **2008**, 887.
[46] S. Herres, A. J. Heuwing, U. Flörke, J. Schneider, G. Henkel, *Inorg. Chim. Acta* **2005**, *358*, 1089.
[47] S. Herres-Pawlis, U. Flörke, G. Henkel, *Eur. J. Inorg. Chem.* **2005**, 3815.
[48] R. Haase, T. Beschnitt, U. Flörke, S. Herres-Pawlis, *Inorg. Chim. Acta* **2011**, *374*, 546.
[49] S. Herres-Pawlis, S. Binder, A. Eich, R. Haase, B. Schulz, G. Wellenreuther, G. Henkel, M. Rübhausen, W. Meyer-Klaucke, *Chem. Eur. J.* **2009**, *15*, 8678.
[50] M. Rohrmüller, A. Hoffmann, C. Thierfelder, S. Herres-Pawlis, W. G. Schmidt, *J. Comput. Chem.* **2015**, *36*, 1672.
[51] C. Citek, J. B. Gary, E. C. Wasinger, T. D. P. Stack, *J. Am. Chem. Soc.* **2015**, *137*, 6991.
[52] C. Citek, S. Herres-Pawlis, T. D. P. Stack, *Acc. Chem. Res.* **2015**, *48*, 2424–2433.
[53] A. P. Cole, V. Mahadevan, L. M. Mirica, X. Ottenwaelder, T. D. P. Stack, *Inorg. Chem.* **2005**, *44*, 7345.
[54] P. Kang, E. Bobyr, J. Dustman, K. O. Hodgson, B. Hedman, E. I. Solomon, T. D. P. Stack, *Inorg. Chem.* **2010**, *49*, 11030.
[55] C. Citek, B.-L. Lin, T. E. Phelps, E. C. Wasinger, T. D. P. Stack, *J. Am. Chem. Soc.* **2014**, *136*, 14405.
[56] W. Kantlehner, E. Haug, W. W. Mergen, P. Speh, T. Maier, J. J. Kapassakalidis, H. J. Bräuner, H. Hagen, *Liebigs Ann. Chem.* **1984**, 108.
[57] S. Herres-Pawlis, A. Neuba, O. Seewald, T. Seshadri, H. Egold, U. Flörke, G. Henkel, *Eur. J. Org. Chem.* **2005**, 4879.
[58] E. A. Lewis, W. B. Tolman, *Chem. Rev.* **2004**, *104*, 1047.
[59] S. Mahapatra, J. A. Halfen, E. C. Wilkinson, G. Pan, X. Wang, V. G. Young Jr., C. J. Cramer, L. Que Jr., W. B. Tolman, *J. Am. Chem. Soc.* **1996**, *118*, 11555.
[60] S. Mahapatra, J. A. Halfen, W. B. Tolman, *J. Am. Chem. Soc.* **1996**, *118*, 11575.
[61] R. Beckert, E. Fanghänel W. D. Habicher, H.-J. Knölker, P. Metz, K. Schwetlick, *Organikum*, Wiley-VCH, Weinheim, Germany, **2009**.
[62] J. Börner, I. dos Santos Vieira, M. D. Jones, A. Döring, D. Kuckling, U. Flörke, S. Herres-Pawlis, *Eur. J. Inorg. Chem.* **2011**, 4441.
[63] M. Kawahata, K. Yamaguchi, T. Ito, T. Ishikawa, *Acta Crystallogr., Sect. E* **2006**, *62*, o3301.
[64] D. Emeljanenko, A. Peters, N. Wagner, J. Beck, E. Kaifer, H.-J. Himmel, *Eur. J. Inorg. Chem.* **2010**, 1839.
[65] S. I. Gorelsky, *SWizard*, http:/www.sg-chem.net.
[66] M. J. Henson, P. Mukherjee, D. E. Root, T. D. P. Stack, E. I. Solomon, *J. Am. Chem. Soc.* **1999**, *121*, 10332.
[67] S. I. Gorelsky, AOMix: Program for Molecular Orbital Analysis, http://www.sg-chem.net/.
[68] S. I. Gorelsky, S. Ghosh, E. I. Solomon, *J. Am. Chem. Soc.* **2006**, *128*, 278.
[69] IUPAC definition: P. Muller, *Pure Appl. Chem.* **1994**, *66*, 1077–1184.
[70] G. J. Kubas, B. Monzyk, A. L. Crumblis, *Tetrakis(acetonitrile) copper(I) Hexafluorophosphate*, in: *Inorganic Syntheses* (Ed.: D. F. Shriver), John Wiley & Sons, Inc., Hoboken, NJ, USA, **1979**, vol. 19, p. 90–92.
[71] M. J. Frisch, G. W. Trucks, H. B. Schlegel, G. E. Scuseria, M. A. Robb, J. R. Cheeseman, J. A. Montgomery Jr., T. Vreven, K. N. Kudin, J. C. Burant, J. M. Millam, S. S. Iyengar, J. Tomasi, V. Barone, B. Mennucci, M. Cossi, G. Scalmani, N. Rega, G. A. Petersson, H. Nakatsuji, M. Hada, M. Ehara, K. Toyota, R. Fukuda, J. Hasegawa, M. Ishida, T. Nakajima, Y. Honda, O. Kitao, H. Nakai, M. Klene, H. Li, J. E. Knox, H. P. Hratchian, J. B. Cross, V. Bakken, C. Adamo, J. Jaramillo, R. Gomperts, R. E. Stratmann, O. Yazyev, A. J. Austin, R. Cammi, C. Pomelli, J. W. Ochterski, P. Y. Ayala, K. Morokuma, G. A. Voth, P. Salvador, J. J. Dannenberg, V. G. Zakrzewski, S. Dapprich, A. D. Daniels, M. C. Strain, O. Farkas, D. K. Malick, A. D. Rabuck, K. Raghavachari, J. B. Foresman, V.

Ortiz, Q. Cui, A. G. Baboul, S. Clifford, J. Cioslowski, B. B. Stefanov, G. Liu, A. Liashenko, P. Piskorz, I. Komaromi, R. L. Martin, D. J. Fox, T. Keith, M. A. Al-Laham, C. Y. Peng, A. Nanayakkara, M. Challacombe, P. M. W. Gill, B. Johnson, W. Chen, M. W. Wong, C. Gonzalez, J. A. Pople, *Gaussian 03*, revision E.01, Gaussian, Inc., Wallingford CT, **2004**.

[72] F. Weinhold, C. Landis, *Valency and Bonding – A Natural Bond Orbital Donor-Acceptor Perspective*, Cambridge University Press, New York, **2005**.

[73] C. J. Cramer, *Essentials of Computational Chemistry: Theories and Models*, Wiley, Chichester, UK, **2004**.

Received: August 5, 2015
Published Online: October 22, 2015

